# Ligand-Assisted Solid-State Transformation of Nanoparticles

Bo Li<sup>[a][b]</sup>, Jinxing Chen<sup>[a][d]</sup>, Lili Han<sup>[c]</sup>, Yaocai Bai<sup>[a]</sup>, Qingsong Fan<sup>[a]</sup>, Chaolumen Wu<sup>[a]</sup>, Xiaojing Wang<sup>[a]</sup>, Michael Lee<sup>[a]</sup>, Huolin L. Xin<sup>[c]</sup>, Zhiwu Han<sup>[b]</sup>, Yadong Yin<sup>[a],\*</sup>

- [a] Department of Chemistry, University of California, Riverside, Riverside, CA 92521, USA
- [b] Key Laboratory of Bionic Engineering (Ministry of Education, China), Jilin University, Changchun, Jilin 130022, P. R. China
- [c] Department of Physics and Astronomy, University of California, Irvine, CA 92697, USA
- [d] Institute of Functional Nano & Soft Materials (FUNSOM), Jiangsu Key Laboratory for Carbon-Based Functional Materials & Devices, Soochow University, Suzhou, Jiangsu 215123, P.R. China

**ABSTRACT**: Thermal treatment is generally a desirable process to improve the properties of nanomaterials, which however often leads to undesirable problems such as aggregation and shape deformation. Here, we overcome this challenge by developing a ligand-assisted calcination strategy for shape-preserved chemical transformation of nanostructures. While capping ligands are often thought to be effective in solution phase synthesis, we show that their presence during high-

temperature calcination not only maintains the overall particle morphology but also offers the possibility of effective creation of controllable porosity in metal oxide nanostructures. We demonstrate a particularly elegant example of this strategy, which involves the chemical conversion of β-FeOOH ellipsoids into porous α-Fe<sub>2</sub>O<sub>3</sub> and magnetic Fe<sub>3</sub>O<sub>4</sub> ellipsoids with morphological preservation and excellent solution dispersity *via* stabilization with strong coordinating capping ligands. The ligand-assisted solid-state conversion strategy represents a general self-templating method for creating nanomaterials, as confirmed by its successful application to a wide range of morphologies (ellipsoids, rods, cubes, and plates) and compositions (hydroxides and metal-organic frameworks).

# 1. INTRODUCTION

Thermal treatment is a general method to improve physical properties of materials by changing their chemical compositions, morphologies, and crystal structures. <sup>1-7</sup> For nanostructured materials, however, heating at a relatively high temperature usually leads to undesirable aggregation, sintering, and significant change to their original morphologies, resulting in the loss of their nanostructural characteristics. Although this morphological change might be valuable in creating new structures in some cases, it is often hoped to maintain their original particle morphology. <sup>8-10</sup> To this end, conventionally, the precursor nanoparticles are coated with a protective physical shell, such as silica, to prevent the nanoparticles from interparticle sintering and aggregation during the heat treatment process. <sup>11-17</sup> However, although the physical shell may maintain the overall particle morphology during calcination, it has little effect on controlling the internal crystal structures, which often leads to the formation of large crystal domains inside. This drastic morphological

deformation significantly decreases effective surface area and affects the chemical properties of nanoparticles. Further, additional steps are required to remove the hard templates after the calcination, e.g. etching with NaOH, which can potentially destroy the nanoparticles or affect their surface properties.

Capping ligands have shown their effectiveness in preserving the morphology of the nanostructures during their chemical transformation in the solution phase. <sup>18, 19, 20</sup> However, the temperature of solution-phase transformation is typically below 300 °C as limited by the boiling point of the solvents, which leads to a low reaction rate and insufficient change in crystallinity and/or phase. Herein, using the chemical conversion of β-FeOOH nanostructures into α-Fe<sub>2</sub>O<sub>3</sub> and magnetic Fe<sub>3</sub>O<sub>4</sub> phases as an example, we report that polymeric ligands can effectively assist the solid-state transformation of nanostructures at elevated temperatures. The ligand-assisted heat treatment method allows successful phase transformation of nanostructures with well-maintained overall morphology, producing new nanostructures with excellent dispersibility in water. The strong coordinating interaction between the capping ligands and nanostructure surface not only provides an opportunity for preventing the fusion of internal grains and attaining solid-state ligand-assisted protection, but more interestingly, enhances the resistance of the capping ligands toward high-temperature degradation.

#### 2. EXPERIMENTAL SECTION

**2.1. Materials and reagents.** Polyacrylic acid (PAA, average M.W. 1800), poly(vinylpyrrolidone) (PVP, Mw=40,000), poly(vinylpyrrolidone) (PVP, Mw=55,000), iron(III) chloride hexahydrate, cetyltrimethylammonium chloride (CTAC), polystyrene sulfonate sodium salt, polyallylamine, hexamethylenetetramine, cobalt(II) chloride hexahydrate, nickel(II) nitrate

hexahydrate were purchased from Sigma-Aldrich. Potassium ferricyanide, hydrochloric acid and ammonium hydroxide (NH<sub>3</sub>·H<sub>2</sub>O, 28% by weight in water) were purchased from Fisher Scientific. Ethanol (200 proof) was purchased from Deco Laboratories Inc. All chemicals were directly used without further purification.

- 2.2. PAA surface modification on the β-FeOOH ellipsoids, β-FeOOH nanorods, Prussian blue nanocubes, Co(OH)<sub>2</sub> nanoplates and Ni(OH)<sub>2</sub> nanoplates. 2 ml NH<sub>3</sub>·H<sub>2</sub>O was added to 40 ml 0.1 M PAA firstly, which was called the A solution. After stirring for about 5 min, 25 ml β-FeOOH ellipsoids/β-FeOOH nanorods/Ni(OH)<sub>2</sub> nanoplates solution was added to the A solution mentioned above in order to obtain the B solution. Then the B solution was heated at 60 °C for about 24h. (PAA modification could also be carried out at room temperature, but it will take a relatively long time). For the PAA modification of Prussian blue nanocubes and Co(OH)<sub>2</sub> nanoplates, except for the absence of ammonia, the others are the same as the methods mentioned above. After the PAA modification process, the product was firstly centrifuged at 11000 rpm for 5 min to remove the excess PAA. Afterward, the particles were washed with water several times and were concentrated in 25 mL water for future use.
- **2.3. Surface protected conversion** *via* heat treatment. For the calcination process, the aqueous solution containing the PAA-modified nanoparticles was dried in an oven at 60 °C to obtain solid sample powders. Then, the solid sample powders were placed in a quartz boat and calcined in a muffle furnace with an air atmosphere. For the reduction process, the sample is pretreated in the same way. The difference is that the quartz boat containing the solid sample powders was placed in the tube furnace with a forming gas (5%  $H_2$  and 95%  $N_2$ ) atmosphere.
- **2.4.** Characterization. Transmission electron microscopy (TEM) images were taken with a Philips Tecnai 12 transmission electron microscope operating at 120 kV. The aberration-corrected

TEM (FEI Titan 80-300) with a fast-responding charge-coupled device (CCD) camera was also used for in situ observation of the morphological evolution process of  $\beta$ -FeOOH ellipsoids with the help of real-time imaging and ED sampling. The samples for TEM observation were prepared by drop-casting a solution on a carbon film supported on a copper grid. The crystal phases of the products were examined with X-ray diffraction (EMPYREAN, PANalytical), in a range of  $2\theta$  from  $10^{\circ}$  to  $80^{\circ}$ . All Fourier transform infrared (FTIR) spectra were performed by Brucker Alpha FT-IR spectrometer in the powder form. Magnetic properties were measured at room temperature using a physical property measurement system (PPMS, PPMS-9T, Quantum Design) with a maximum applied field of 45 kOe.

## 3. RESULTS AND DISCUSSION

The overall chemical transformation process involves first wrapping akaganéite (β-FeOOH) nanostructures with polymeric ligands and subsequent heat treatment to produce porous iron oxide phases (Figure 1a). The ellipsoidal β-FeOOH nanostructures were obtained from the hydrolysis of diluted aqueous iron chloride (FeCl<sub>3</sub>·6H<sub>2</sub>O) solution (Figure S1). A layer of polymeric ligands was then introduced onto the nanoparticle surface by solution-phase incubation, <sup>20</sup> and then calcined in air to initiate phase transformation. Here polyacrylic acid (PAA) with a molecular weight of 1800 was employed as a model ligand in the ligand-assisted conversion due to the strong coordination between the iron cation and carboxyl group.<sup>18</sup>

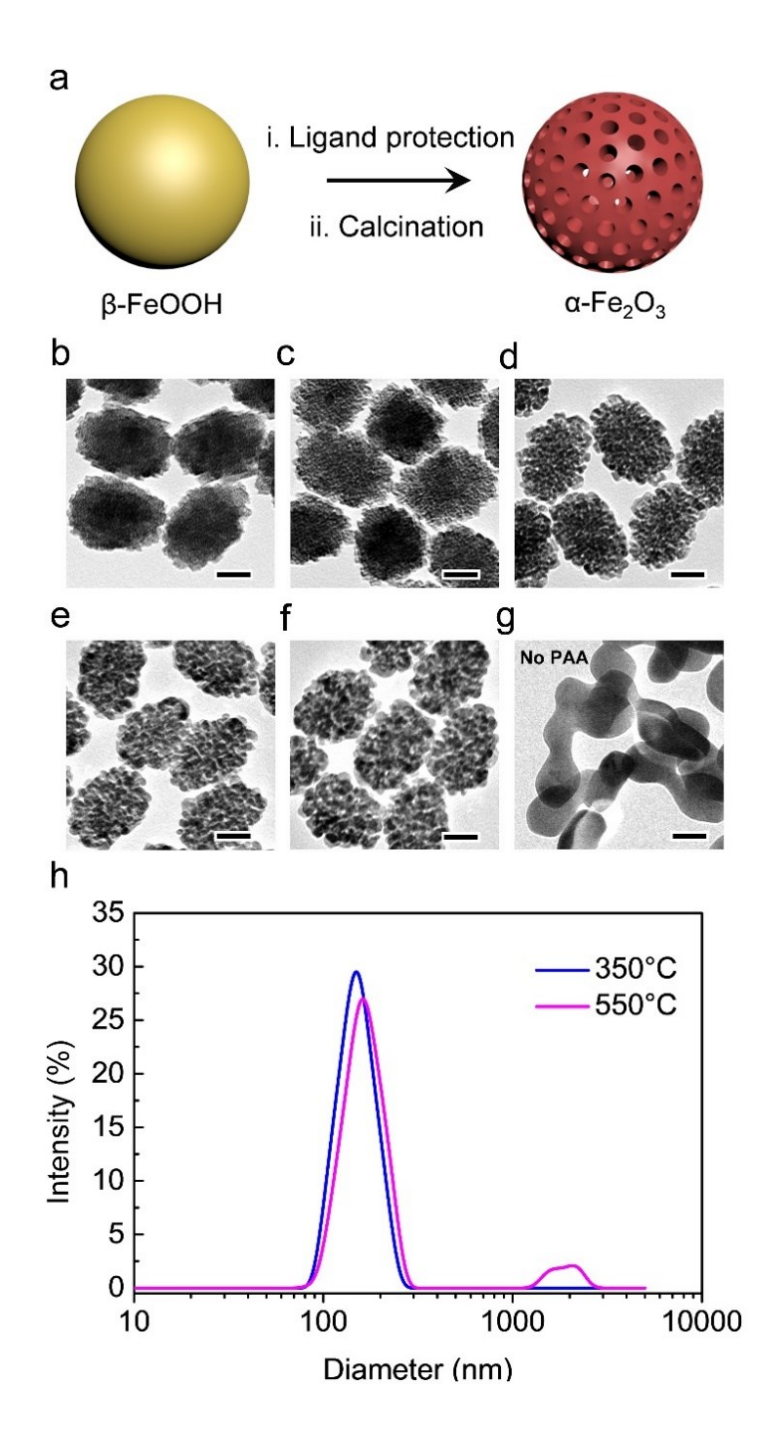


**Figure 1: a**, schematic illustration of the ligand-assisted solid-state transformation process in air. **b-f**, TEM images of the PAA-modified ellipsoids after calcination for 2h at a gradient temperature from 150 °C to 550 °C with an interval of 100 °C. **g**, the ellipsoids without PAA protection calcined at 550 °C for 2h. Scale bars: 50 nm. **h**, the size distributions of PAA-modified ellipsoids calcined for 2h at 350 °C and 550 °C, respectively.

Figures 1b-f show the transmission electron microscopy (TEM) images of the PAA-modified β-FeOOH ellipsoids calcined in air for 2 h at 150 °C, 250 °C, 350 °C, 450 °C and 550 °C, respectively. It could be found that these calcined nanoparticles still maintained the ellipsoidal morphology, formed porous nanostructures, and possessed a good dispersibility in water (Figure S2). With the rising of annealing temperature, both the pore size and domain size of ellipsoids increased significantly (Figure S3) while the specific surface area decreased rapidly (Figure S4). On the contrary, the β-FeOOH ellipsoids without PAA lost their original shape and were converted into a monocrystalline lamellar structure, which fused during the chemical transition (Figure 1g). For the β-FeOOH ellipsoids calcined at 350 °C, the hydrodynamic radius with distribution in a narrow diameter range was similar to those measured from TEM images, indicating that the ellipsoids calcined at 350 °C dispersed as separate particles in water (blue line in Figure 1h and Figure S5). Even after calcination at 550 °C, over 94% of the ellipsoids remain as individual particles (pink line in Figure 1h). The hydrodynamic radius of a tiny fraction of ellipsoids dramatically increased, indicating modest interparticle aggregation. We further increased the heating temperature to 600 °C and 650 °C to find out the temperature limit at which the ligand would lose its protective effect. For the ellipsoids calcined at 600 °C, the overall morphology, porous nanostructures, and their water dispersity were well maintained, as shown in Figures S6a and b. However, the particles calcined at 650 °C showed a severe aggregation (Figures S6c and d) with their original boundaries indistinguishable, suggesting the loss of sufficient protection due to the decomposition of ligands at such a high temperature. In addition, severe aggregation could occur if the sample previously treated at 550 °C was re-calcined for 2h at the same temperature, indicating the lack of long-term stability of the ligands under this condition. However, if the pre-treated particles were modified

with PAA again, then they could maintain their overall ellipsoidal morphology and porous structures after second-round calcination, as shown in Figure S7.

With the help of real-time HAADF-STEM imaging, we were able to directly observe the morphological evolution of β-FeOOH ellipsoids during their heat treatment. Interestingly, at a much higher heating rate inside the microscope than in the oven, the PAA-modified β-FeOOH ellipsoids were able to maintain their morphology at temperatures up to 700 °C. Figures 2a-d show a TEM image of the particles calcined at 700 °C and the corresponding elemental mapping, indicating the homogeneous distribution of Fe and O elements. As shown in Figure 2e, upon annealing from room temperature to 700 °C at 10 °C/min, the PAA-modified β-FeOOH ellipsoids showed no apparent microstructural change at a low temperature, but above 200 °C some porosity started to develop due to the dehydration reaction of β-FeOOH and the merger of the small crystallites inside these particles. Throughout the process, the pore size increased gradually and the external dimension of the ellipsoids decreased. As a control experiment, Figure 2f shows the morphology evolution of the nanoparticles without PAA protection during the calcination process. With the increase of temperature, their pore size increased at a much higher rate than that of PAAmodified ones. At 700 °C, they showed significant sintering while those with PAA protection could still maintain their overall morphology and the exquisite porous structure.

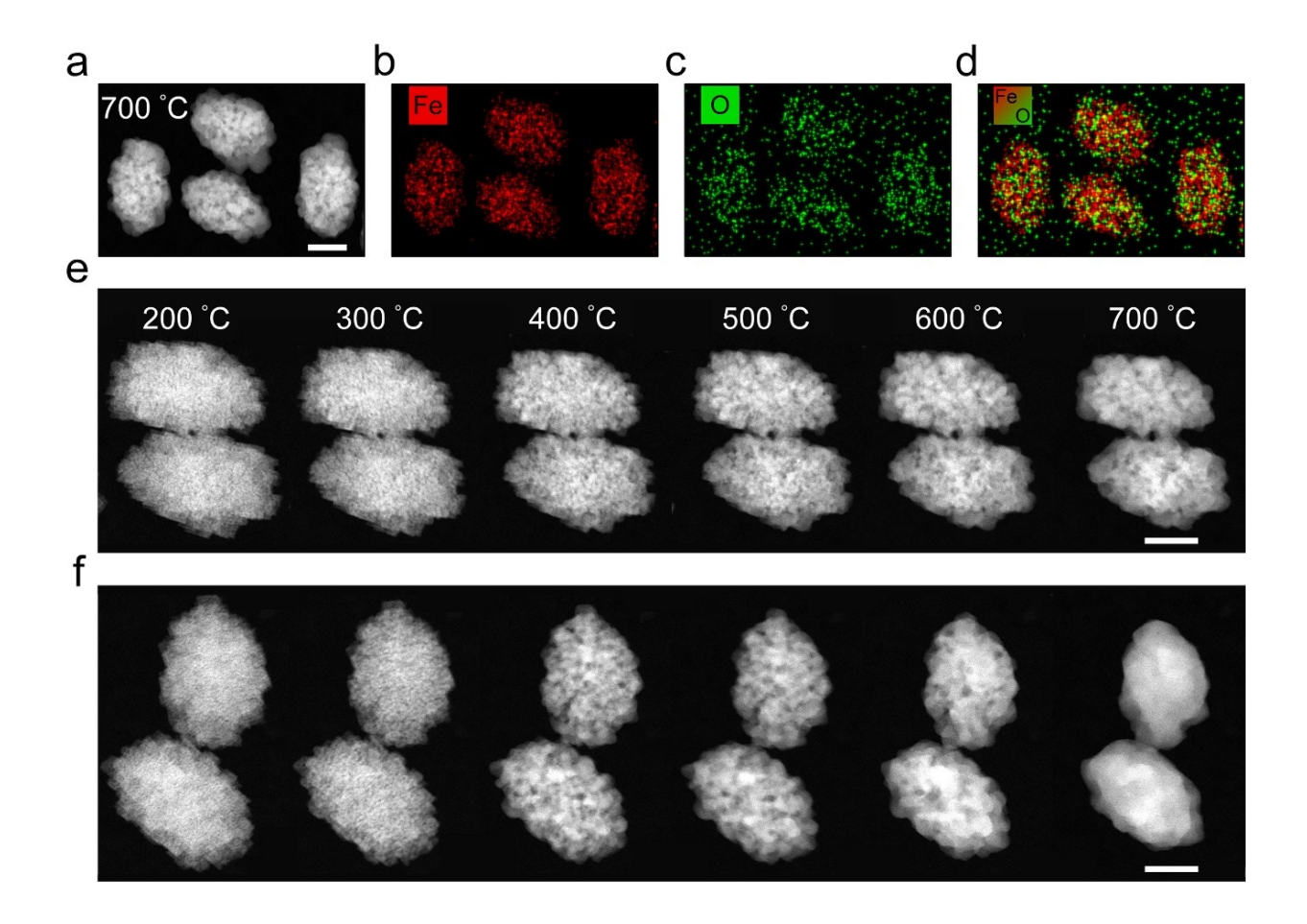


**Figure 2: a-d**, TEM image of PAA-modified ellipsoids calcined at 700 °C and corresponding elemental mapping images of Fe and O in the same area. **e**, **f**, *in situ* TEM images of β-FeOOH ellipsoids modified with and without PAA, respectively. Scale bars: 50 nm.

As the size of capping ligands is expected to greatly influence their binding affinity and high-temperature tolerance, we studied the protective effect of PAA with different molecular weights (5000 and 100,000) on the transformation of β-FeOOH ellipsoids upon 2h calcination at 600 °C. Compared with the previous one with a molecular weight of 1800, PAA with a molecular weight of 5000 could not only prevent ellipsoids from large shape deformation but also maintain a better dispersibility in water (Figures S8a and b). In addition, the domain size was also significantly smaller than that shown in Figure S6a where nanoparticles were modified by PAA with a

molecular weight of 1800. For PAA with a significantly larger molecular weight (100,000), however, the porous nanostructures were almost completely destroyed and the domain size became relatively large. Also, the edges of the ellipsoids contacted and even fused, resulting in severe agglomerations. It is believed that when the molecular weight of the PAA is too high, the steric repulsion between polymer chains increases significantly, which reduces the amount of the polymer chains attached to the particle surfaces. In addition, the steric hindrance within a large macromolecule also allows fewer carboxyl groups to be bound to the FeOOH surface. As a result, the effective protection against grain growth and interparticle fusion is limited for large polymers, which has been confirmed by performing thermal gravimetric analysis results, as shown in Figure S9.

To identify the species during the heat treatment of nanoparticles, the ellipsoids were annealed for 2 h at a gradient temperature from 250 °C to 550 °C with an interval of 100 °C. At room temperature, X-ray diffraction (XRD) pattern shows multiple diffraction peaks corresponding to  $\beta$ -FeOOH (Figure 3a). Standard patterns of  $\beta$ -FeOOH (JCPDS card 34-1266),  $\gamma$ -Fe<sub>2</sub>O<sub>3</sub> (JCPDS card 25-1402) and  $\alpha$ -Fe<sub>2</sub>O<sub>3</sub> (JCPDS card 33-0664) are shown for comparison. If the calcination temperature was increased to 250 °C, the corresponding pattern demonstrates that the chemical composition of the ellipsoids changes entirely. The porous products remained primarily amorphous even after calcination at 450 °C. However, very weak and broad peaks were observed at 20 = 35°, 55° and 63°, indicating the existence of an iron-vacancy phase ( $\gamma$ -Fe<sub>2</sub>O<sub>3</sub>) with a very small crystal size. When the calcination temperature reached 470 °C (Figure S10), the main composition of the porous nanoparticles became  $\alpha$ -Fe<sub>2</sub>O<sub>3</sub>. The XRD patterns show an increasing intensity of  $\alpha$ -Fe<sub>2</sub>O<sub>3</sub> diffraction peaks, with  $\alpha$ -Fe<sub>2</sub>O<sub>3</sub> emerging as the sole species at 550 °C, as shown in Figures 3a, S10 and S11.

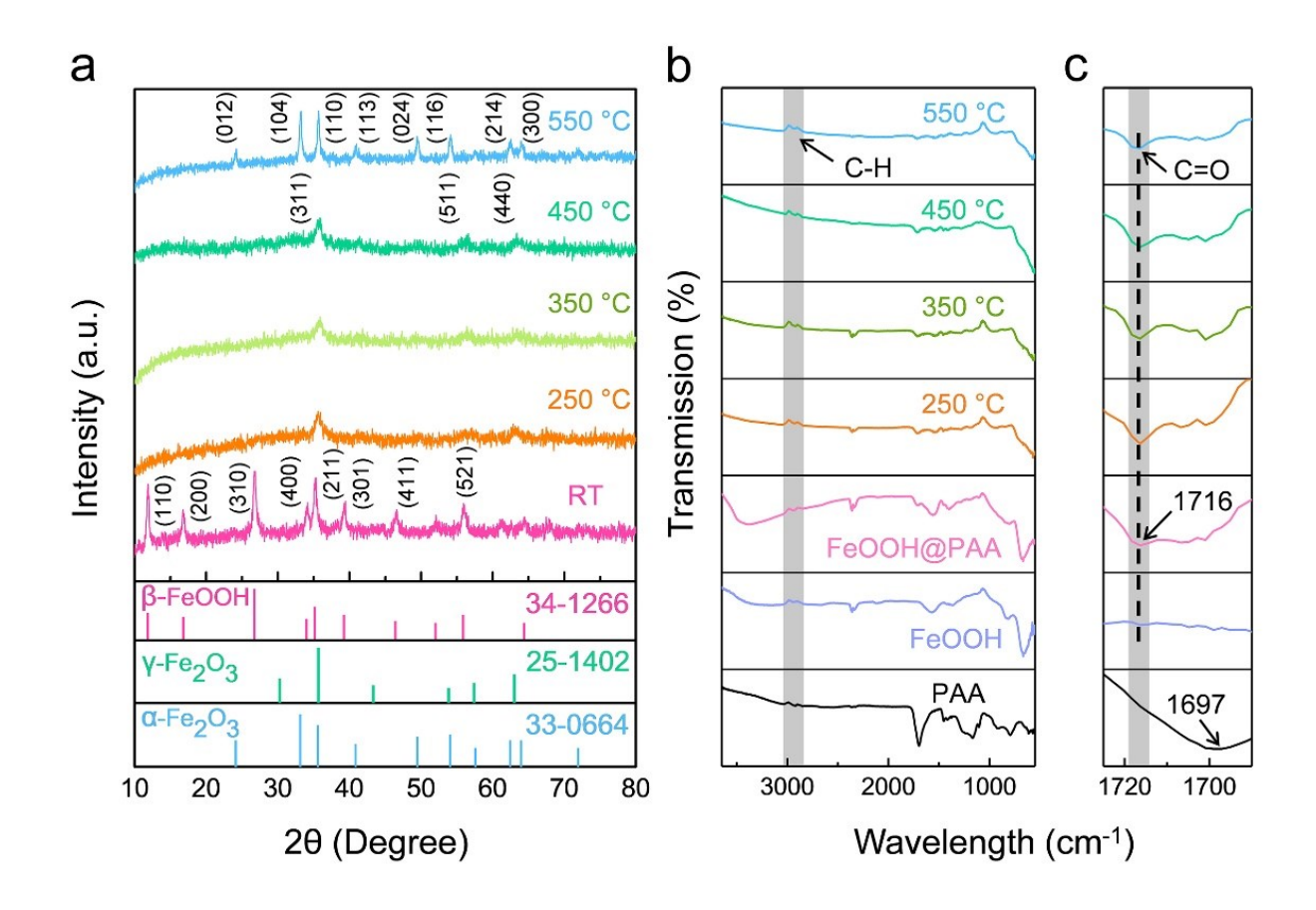


Figure 3: a, XRD patterns showing the phase transformation process of β-FeOOH ellipsoids prepared under various calcination temperatures for 2h. b and c, FTIR spectrum proving the existence of PAA which protected ellipsoids during the heat treatment process.

To further clarify the protective effect of the polymeric ligand, we used Fourier transform infrared spectroscopy (FTIR) to analyze the chemical bonds of the pure PAA,  $\beta$ -FeOOH, PAA-modified  $\beta$ -FeOOH, and PAA-modified  $\beta$ -FeOOH calcined at various temperatures. As shown in the gray area of Figure 3b, the weak absorption peaks at 2986 and 2905 cm<sup>-1</sup> were assigned to the stretching vibration of the C-H bond, which could prove the presence of alkyl groups in all of the tested nanoparticles. Figure 3c is a local, enlarged drawing of Figure 3b with a range from 1690 to 1725 cm<sup>-1</sup>. The peak at 1716 cm<sup>-1</sup> was assigned to the stretching vibration of the carbon-oxygen

double bond, which could only be provided by PAA. The blue curve proved that there were still C=O bonds existing on the surface of ellipsoids even at 550 °C. Therefore, we could deduce that carboxyl groups of PAA still combined with ellipsoids at relatively high temperatures. Through the strong coordination interaction between the iron cations and multiple carboxyl groups, PAA acted as a multidentate ligand on the surface of the nanoparticles, preventing the particles from breaking down. It is worth noting that, for the β-FeOOH particles without PAA modification, the C=O bond characteristic peaks were not found on the FTIR spectrum, which was consistent with the sintering behavior shown in Figure 2f.

After understanding the protective role of PAA, it is also interesting to study the role of other ligands in high-temperature solid-state transformation. FeOOH ellipsoids were modified by polystyrene sulfonate sodium salt (PSS), polyallylamine, and polyvinylpyrrolidone (PVP) and then calcined for 2h at 350 °C and 550 °C. PSS was chosen as it was a typical ionic ligand with a weak coordination group of -SO<sub>4</sub><sup>-</sup> to iron cations. While polyallylamine bound to β-FeOOH strongly through the coordination interaction of amine to iron cations, PVP only bound weakly. At 350 °C, all three ligands demonstrated sufficient capability in suppressing the morphological deformation of the nanoparticles (Figure S12). At 550 °C, however, all three cases showed significant grain growth (Figure S13). The only difference was that the particles modified by polyallylamine could be well dispersed in water while the other two samples were severely aggregated. This result was consistent with the stronger binding of polyallylamine than the other two ligands on the β-FeOOH surface, which prevented interparticle fusion. However, unlike the negatively charged PAA, polyallylamine was positively charged and its initial binding to the positively charged β-FeOOH surface was limited. As a result, polyallylamine molecules of insufficient amounts were not able

to efficiently prevent the grain growth of  $\beta$ -FeOOH during the calcination process, although they blocked the interparticle fusion.

This ligand-assisted strategy is general and can be applied to the high-temperature solid-state transformation of a variety of nanomaterials, including not only β-FeOOH ellipsoids, but also β-FeOOH nanorods, Prussian blue (PB) nanocubes, cobalt hydroxide (Co(OH)<sub>2</sub>) nanoplates, and Ni(OH)<sub>2</sub> nanoplates. Figure 4a shows the morphology evolution of β-FeOOH rods during calcination at various temperatures for two hours. As the heating temperature increased, the dehydration reaction proceeded further. The voids formed inside the rods became larger and larger, eventually leading to the formation of capsule-like α-Fe<sub>2</sub>O<sub>3</sub> nanorods with good waterdispersibility (Figures S14 and S15). By contrast, the nanorods without PAA modification underwent drastic morphological changes and severe aggregation (Figure 4b). Similarly, PB nanocubes also underwent chemical transformations when heated in air at 350 °C for 2h, becoming γ-Fe<sub>2</sub>O<sub>3</sub> nanocubes (Figures 4c, d and g).<sup>22</sup> Their nanostructures retained original shapes and water dispersibility but had additional porosity. In contrast, if PB cubes were not modified by PAA, most cubes decompose into much smaller pieces after calcination (Figures S16a and c). Even reducing the calcination temperature to 250 °C could not keep the original cube shape (Figures S16b and d). The ligand-protection also worked on the conversion of metal hydroxide nanoplates such as Co(OH)<sub>2</sub> and Ni(OH)<sub>2</sub> which can be converted into Co<sub>3</sub>O<sub>4</sub> (Figures 4f and h) and Ni<sub>2</sub>O<sub>3</sub> (Figure S17) porous nanoplates with well-maintained original morphologies. These examples clearly demonstrated that the ligand-assisted conversion procedure could be regarded as a universal strategy for the chemical transformation of nanostructures.

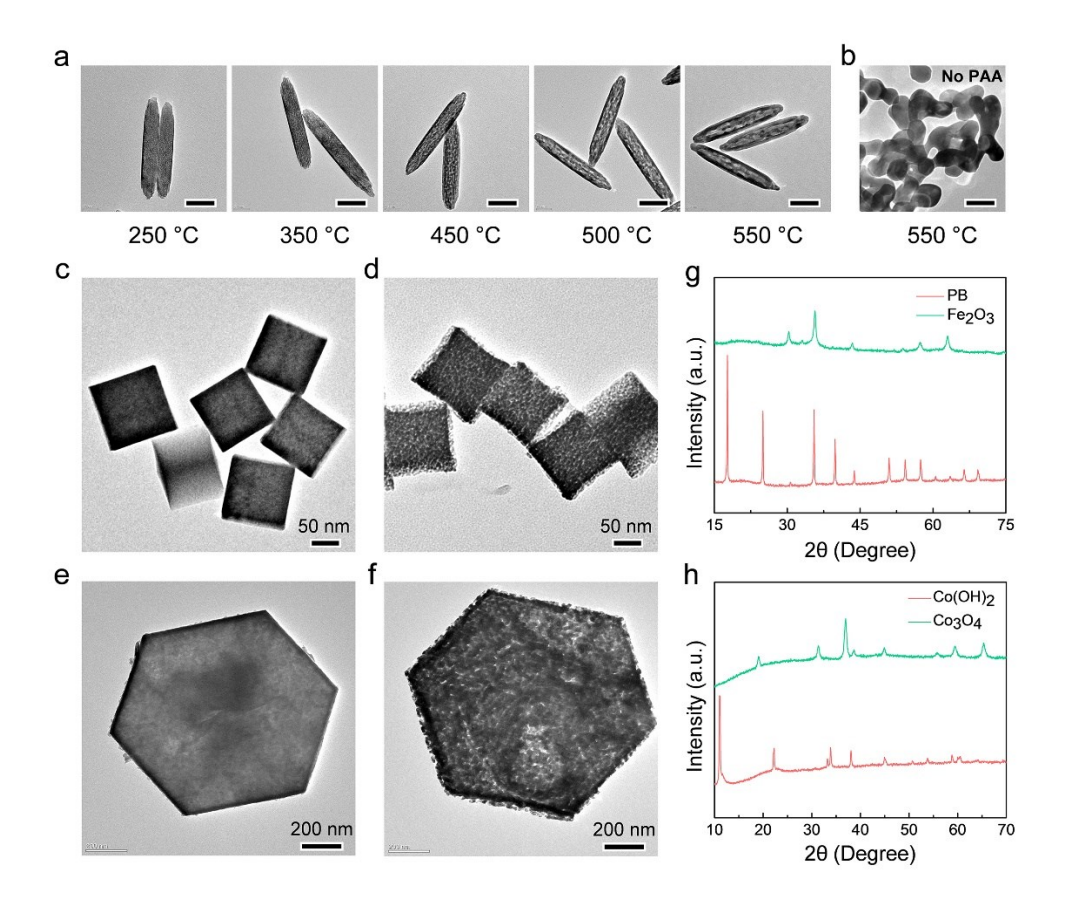


**Figure 4: a**, TEM images about the PAA-modified β-FeOOH rods calcined at a set of temperature. Scale bars: 100 nm. **b**, β-FeOOH rods without PAA calcined at 550 °C for 2h. Scale bar: 100 nm. **c-f**, TEM images of PB nanocubes and Co(OH)<sub>2</sub> nanoplates before (**b** and **d**) and after (**c** and **e**) ligand-assisted calcination. **g** and **h**, the corresponding XRD patterns to the samples at left.

An important advantage of the ligand-assisted strategy is that it can be conveniently applied in multi-step solid-state transformation processes to avoid the undesired drastic morphological and structural changes that often occur when multiple reactions are triggered in a one-step process. Taking magnetite (Fe<sub>3</sub>O<sub>4</sub>) as an example, while its nanostructures are highly desirable for many technological applications such as biosensors and bioimaging, their direct synthesis with well-defined morphologies and high water dispersity is rather challenging. Here we show that the ligand-assisted strategy can be employed to produce Fe<sub>3</sub>O<sub>4</sub> nanoscale ellipsoids and rods from their

corresponding β-FeOOH precursors, by first dehydration and then a reduction reaction (Figure 5a). The reduction process was divided into two steps. In the first step, the β-FeOOH ellipsoids and rods were modified by PAA and then calcined at 330 °C in air to induce dehydration reaction, producing porous Fe<sub>2</sub>O<sub>3</sub> ellipsoids and rods (Figures 5b and d). In the second step, the porous ellipsoids and rods were modified with PAA again and then reduced at 330 °C in the forming gas (5% H<sub>2</sub> and 95% N<sub>2</sub>) to produce the Fe<sub>3</sub>O<sub>4</sub> phase (Figures 5c and e). The transformation from β-FeOOH to Fe<sub>3</sub>O<sub>4</sub> has been confirmed by XRD analysis (Figures 5f and h). The secondary modification with PAA complemented the PAA consumed in the first step. The advantage of this method was that the nanoparticles were only reduced in the second stage without a simultaneous dehydration reaction. Simultaneous dehydration and reduction reactions could lead to drastic changes in the morphologies and compositions, destroying the nanoparticles during the chemical transformation process.

A comparative experiment was carried out to verify the necessity of the two-step process. The nanorods with PAA modification were reduced directly at 330 °C in forming gas. As shown in Figure S18, the edge of the nanorods was damaged at multiple sites and no clear porous nanostructure was formed inside the rods. The morphology loss was most likely due to the significant structural rearrangement associated with the extensive crystallization and grain growth during the dehydration and reduction reactions. It was also necessary to perform secondary PAA modification before the reduction in the second step. When the porous Fe<sub>2</sub>O<sub>3</sub> ellipsoids obtained in the first step were directly reduced, although particles could be partially converted into porous Fe<sub>3</sub>O<sub>4</sub> magnetic nanoparticles, a considerable part of the Fe<sub>2</sub>O<sub>3</sub> ellipsoids fused during the reduction process (Figure S19). This may be due to that a large amount of PAA was consumed in the first step and there was insufficient PAA to protect the nanoparticles during reduction.

Figures 5g and 5i show the hysteresis loops measured at room temperature, demonstrating magnetic properties of the Fe<sub>3</sub>O<sub>4</sub> ellipsoids and rods. The porous Fe<sub>3</sub>O<sub>4</sub> nanoparticles showed nonlinear magnetization curves, which excluded the existence of pure paramagnetism. Their room temperature magnetization curves saturated at a low magnetic field, indicating that they could show a quick response to the externally applied magnetic field. Both samples showed a small remanent magnetization ( $M_r$ ) and coercive force ( $H_c$ ), with saturation magnetization ( $M_s$ ) of 33 and 32 em $\mu \cdot g^{-1}$  for Fe<sub>3</sub>O<sub>4</sub> ellipsoids and rods, respectively.<sup>23, 24</sup>

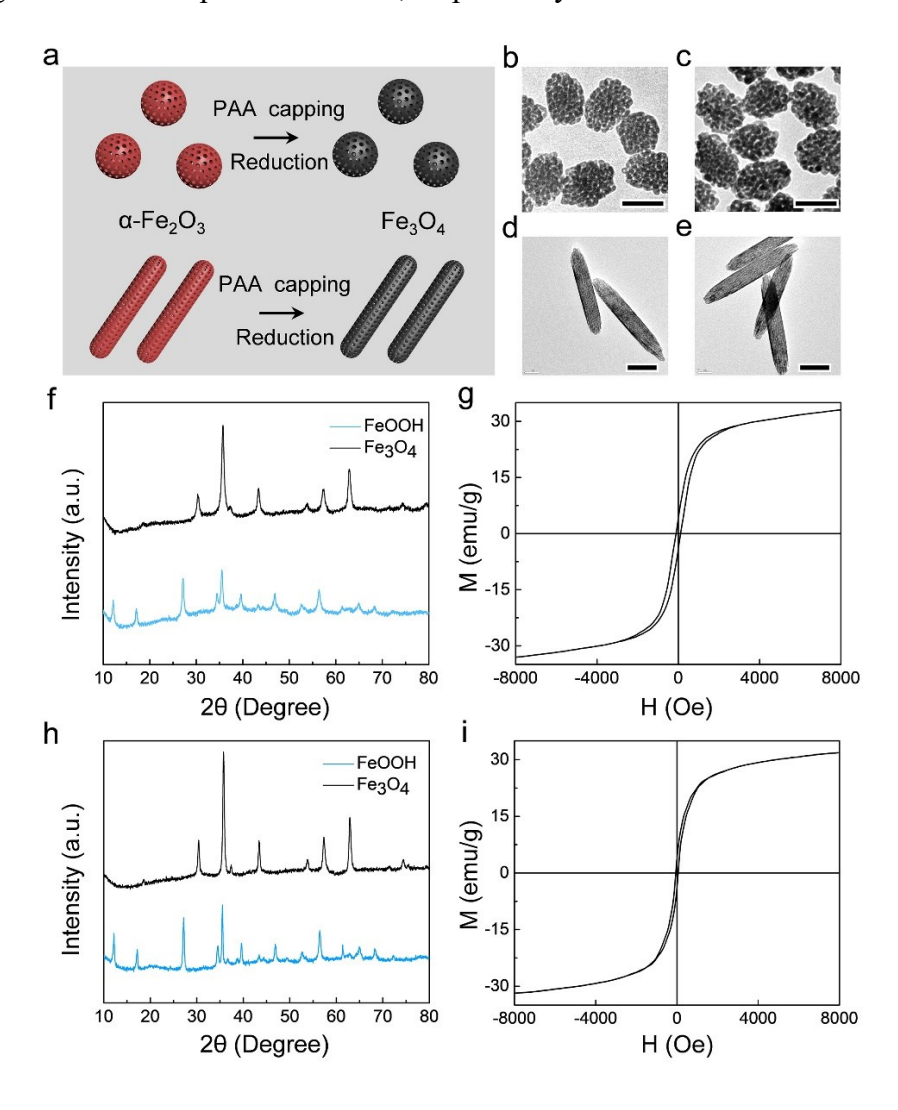


**Figure 5: a**, Schematic illustrations of ligand-assisted reduction process in forming gas. **b-e**, TEM images of β-FeOOH ellipsoids and nanorods before (**b** and **d**) and after (**c** and **e**) ligand-assisted

reduction. **f** and **h** are the XRD patterns corresponding to the ellipsoids (**b** and **c**) and nanorods (**d** and **e**), respectively. **g** and **i**, magnetic hysteresis loops of synthesized Fe<sub>3</sub>O<sub>4</sub> ellipsoids and nanorods. Scale bars: 100 nm.

## 4. CONCLUSIONS

In summary, we have shown that polymeric capping ligands can effectively suppress the morphological deformation of nanoparticles during their high-temperature solid-state chemical transformation. Using  $\beta$ -FeOOH ellipsoids as an example, we demonstrate that ellipsoids modified by strong coordinating capping ligands could enable their successful conversions into porous Fe<sub>2</sub>O<sub>3</sub> and magnetic Fe<sub>3</sub>O<sub>4</sub> ellipsoids with well-maintained overall morphologies during calcination in air and forming gas. This finding refines our understanding of the protection function of capping ligands to nanostructures and expands their effectiveness from conventional solution-phase reaction to high-temperature solid-state transformation. Our strategy is conceptually universal and can be applied to the solid-state transformation of nanostructures of various compositions and morphologies, therefore promoting chemical transformation as a general and powerful tool for the synthesis of nanostructures. Due to the greatly reduced use of solvents and fewer steps, this ligand-assisted solid-state transformation strategy offers great advantages in the manufacture of nanomaterials, such as easy mass production, significantly reduced production costs, and minimal negative impact on the environment.

# ASSOCIATED CONTENT

**Supporting Information**. The Supporting Information is available free of charge on the ACS Publications website.

Details of the experiments, additional TEM images, pore size distribution and surface areas, and XRD characterization of the original and calcined samples.

# **AUTHOR INFORMATION**

# **Corresponding Author**

Yadong Yin (lead contact)

Department of Chemistry, University of California, Riverside, CA 92521, USA

Tel: 951-827-4965

yadong.yin@ucr.edu

# **Author Contributions**

B.L. and J.C. contributed equally. Y.Y., J.C., and B.L. conceived the idea. B.L., J.C., Y.B., Z.H. and H.X. designed the experiments. B.L., L.H., Q.F., C.W. and X.W. performed all of the experiments. The manuscript was written by B.L., J.C., and M.L, and revised by Y.Y. All authors contributed to the general discussion and reviewed the manuscript.

# **Notes**

The authors declare no competing financial interest.

# ACKNOWLEDGMENT

Y.Y. acknowledges the support from the U.S. National Science Foundation (CHE-1808788). B.L. thanks the fellowship support by the China Scholarship Council (CSC). Acknowledgment is also made to the Donors of the American Chemical Society Petroleum Research Fund (55904-ND10) for partial support of this research. This work is also supported by the National Key Research and

Development Program of China (No.2018YFA0703300). J.C. thanks the support from the National Natural Science Foundation of China (51901147) and China Postdoctoral Science Foundation (2019M651939). The authors also thank the Central Facility for Advanced Microscopy and Microanalysis at UCR for help with TEM analysis.

# REFERENCES

- 1. Xia, W.; Yang, Y.; Meng, Q.; Deng, Z.; Gong, M.; Wang, J.; Wang, D.; Zhu, Y.; Sun, L.; Xu, F.; Li, J.; Xin, H. L. Bimetallic nanoparticle oxidation in three dimensions by chemically sensitive electron tomography and in situ transmission electron microscopy. *ACS Nano* **2018**, *12*, 7866-7874.
- 2. Han, L.; Cai, S.; Gao, M.; Hasegawa, J. Y.; Wang, P.; Zhang, J.; Shi, L.; Zhang, D. Selective catalytic reduction of NO<sub>x</sub> with NH<sub>3</sub> by using novel catalysts: State of the art and future prospects. *Chem. Rev.* **2019**, *119*, 10916-10976.
- 3. Wu, H.; Lee, D.; Tufa, L. T.; Kim, J.; Lee, J. Synthesis mechanism of magnetite nanorods containing ordered mesocages. *Chem. Mater.* **2019**, *31*, 2263-2268.
- 4. Oh, M. H.; Yu, T.; Yu, S. H.; Lim, B.; Ko, K. T.; Willinger, M. G.; Seo, D. H.; Kim, B. H.; Cho, M. G.; Park, J. H.; Kang, K.; Sung, Y. E.; Pinna, N.; Hyeon, T. Galvanic replacement reactions in metal oxide nanocrystals. *Science* **2013**, *340*, 964-968.
- 5. Sun, Y.; Xia, Y. Shape-controlled synthesis of gold and silver nanoparticles. *Science* **2002**, 298, 2176-2179.

- 6. Sadtler, B.; Demchenko, D. O.; Zheng, H.; Hughes, S. M.; Merkle, M. G.; Dahmen, U.; Wang, L. W.; Alivisatos, A. P. Selective facet reactivity during cation exchange in cadmium sulfide nanorods. *J. Am. Chem. Soc.* **2009**, *131*, 5285-5293.
- 7. Xia, Y.; Li, W.; Cobley, C. M.; Chen, J.; Xia, X.; Zhang, Q.; Yang, M.; Cho, E. C.; Brown, P. K. Gold nanocages: from synthesis to theranostic applications. *Acc. Chem. Res.* **2011**, *44*, 914-924.
- 8. Chou, N. H.; Schaak, R. E. Shape-controlled conversion of beta-Sn nanocrystals into intermetallic M-Sn (M=Fe, Co, Ni, Pd) nanocrystals. *J. Am. Chem. Soc.* **2007**, *129*, 7339-7345.
- 9. Moon, G. D.; Ko, S.; Xia, Y.; Jeong, U. Chemical transformations in ultrathin chalcogenide nanowires. *ACS Nano* **2010**, *4*, 2307-2319.
- 10. Saruyama, M.; So, Y. G.; Kimoto, K.; Taguchi, S.; Kanemitsu, Y.; Teranishi, T. Spontaneous formation of wurzite-CdS/zinc blende-CdTe heterodimers through a partial anion exchange reaction. *J. Am. Chem. Soc.* **2011**, *133*, 17598-17601.
- 11. Piao, Y.; Kim, J.; Na, H. B.; Kim, D.; Baek, J. S.; Ko, M. K.; Lee, J. H.; Shokouhimehr, M.; Hyeon, T. Wrap-bake-peel process for nanostructural transformation from beta-FeOOH nanorods to biocompatible iron oxide nanocapsules. *Nat. Mater.* **2008**, *7*, 242-247.
- 12. Joo, J. B.; Zhang, Q.; Lee, I.; Dahl, M.; Zaera, F.; Yin, Y. Mesoporous anatase titania hollow nanostructures though silica-protected calcination. *Adv. Funct. Mater.* **2012**, *22*, 166-174.
- 13. Kumar, A.; Jeon, K. W.; Kumari, N.; Lee, I. S. Spatially confined formation and transformation of nanocrystals within nanometer-sized reaction media. *Acc. Chem. Res.* **2018**, *51*, 2867-2879.

- 14. Kwon, T.; Jeon, K.-W.; Dutta, S.; Lee, I. S. Conversion chemistry of nanoscopically confined manganese silicate: Solid-state route toward porous metal oxide catalyst-support. *Chem. Mater.* **2018**, *30*, 8070-8078.
- 15. Wang, X.; Feng, J.; Yu, H.; Jin, Y.; Davidson, A.; Li, Z.; Yin, Y. Anisotropically shaped magnetic/plasmonic nanocomposites for information encryption and magnetic-field-direction sensing. *Research* **2018**, *2018*, 1-13.
- 16. Li, H.; Li, C.; Sun, W.; Wang, Y.; Hua, W.; Liu, J.; Zhang, S.; Chen, Z.; Wang, S.; Wu, Z.; Zhu, Q.; Tang, R.; Yu, J.; He, L.; Ozin, G. A.; Zhang, X. Single-stimulus-induced modulation of multiple optical properties. *Adv. Mater.* **2019**, *31*, e1900388.
- 17. Chen, J.; Feng, J.; Yang, F.; Aleisa, R.; Zhang, Q.; Yin, Y. Space-confined seeded growth of Cu nanorods with strong surface plasmon resonance for photothermal actuation. *Angew. Chem., Int. Ed.* **2019**, *131*, 9376-9382.
- 18. Xu, W.; Wang, M.; Li, Z.; Wang, X.; Wang, Y.; Xing, M.; Yin, Y. Chemical transformation of colloidal nanostructures with morphological preservation by surface-protection with capping ligands. *Nano Lett.* **2017**, *17*, 2713-2718.
- 19. Liu, L.; Gao, Z.; Jiang, B.; Bai, Y.; Wang, W.; Yin, Y. Reversible assembly and dynamic plasmonic tuning of Ag nanoparticles enabled by limited ligand protection. *Nano Lett.* **2018**, *18*, 5312-5318.
- 20. Xu, W.; Lyu, F.; Bai, Y.; Gao, A.; Feng, J.; Cai, Z.; Yin, Y. Porous cobalt oxide nanoplates enriched with oxygen vacancies for oxygen evolution reaction. *Nano Energy* **2018**, *43*, 110-116.

- 21. Yu, L.; Han, R.; Sang, X.; Liu, J.; Thomas, M. P.; Hudak, B. M.; Patel, A.; Page, K.; Guiton, B. S. Shell-induced ostwald ripening: Simultaneous structure, composition, and morphology transformations during the creation of hollow iron oxide nanocapsules. *ACS Nano* **2018**, *12*, 9051-9059.
- 22. Zhang, L.; Wu, H. B.; Madhavi, S.; Hng, H. H.; Lou, X. W. Formation of Fe<sub>2</sub>O<sub>3</sub> microboxes with hierarchical shell structures from metal-organic frameworks and their lithium storage properties. *J. Am. Chem. Soc.* **2012**, *134*, 17388-17391.
- 23. Kitagawa, Y.; Hiraoka, Y.; Honda, T.; Ishikura, T.; Nakamura, H.; Kimura, T. Low-field magnetoelectric effect at room temperature. *Nat. Mater.* **2010**, *9*, 797-802.
- 24. Hu, M.; Belik, A. A.; Imura, M.; Mibu, K.; Tsujimoto, Y.; Yamauchi, Y. Synthesis of superparamagnetic nanoporous iron oxide particles with hollow interiors by using prussian blue coordination polymers. *Chem. Mater.* **2012**, *24*, 2698-2707.

# TOC Graphic:

